ELSEVIER

Polymer 43 (2002) 6839–6851

polymer

www.elsevier.com/locate/polymer

Microstructure evolution in polyamide PA11 under small uniaxial extension

L. Jolly, A. Tidu*, J.-J. Heizmann, B. Bolle

Laboratoire d'Etude des Textures et Application aux Matériaux, UMR CNRS 7078, ISGMP Université de Metz, 57045 Metz-Cedex, France

Received 30 July 2001; received in revised form 19 November 2001; accepted 15 July 2002

Abstract

Polyamide 11 (PA11) is a linear semicrystalline polymer. Bulk samples of PA11 were compression moulded from the melt. The aim of this study is to describe the deformation of the structure during an uniaxial drawing (up to a true strain of 0.4) at room temperature. The structure of the studied samples is described on two scales by two different X-ray scattering techniques. The small angle X-ray scattering (SAXS) method investigates the structure on the scale of lamellae, whereas the wide-angle X-ray scattering (WAXS) method investigates the macromolecular structure. The studied samples are constituted of three macromolecular structures: an amorphous phase (approximately 60 vol%), a crystalline phase called α (≈20 vol%), and a smectic phase called δ' (≈20 vol%). The study of the descriptive parameters of the diffusion peaks shows that lamellae orient themselves weakly towards the drawing direction. The same tendency is observed for the chain segments of the smectic and amorphous phases. On the other hand, the chain segments of the crystalline phase, that constitutes the lamellae, orient themselves strongly perpendicularly to the drawing direction. The comparison between the results from the two investigated scales allows us to propose the activation of a twinning mechanism in the lamellae parallel to the drawing direction.

Keywords: Polyamide; Deformation mechanism; Microstructure analysis

1. Introduction

Among all the semicrystalline polymers of high technological interest, polyamides are widely used polymers with a large range of industrial fields. As for the other semicrystalline polymers, crystallinity (shape, size and perfection of the crystallite, size of the spherulites) and morphological features are the main factors affecting their properties.

Because the end-use properties of these semicrystalline polymers are mainly dependent on their molecular structure and on their mechanical properties, the mechanism of deformation, in relation with the processing variables, is a subject of intense research [1].

The polyamides are divided in different types based on their molecular structure. The most common are polyamides PA6 and PA6,6, and therefore, they are one of the mostly studied. The case of spherulitic semi-crystalline polyamide PA11 (generally used from automotive to offshore applications) is nevertheless not yet well documented. Polyamide can be obtained with markedly different chain structure and physical/chemical properties by varying the polymerisation process and/or by changing the thermo-mechanical treatment.

Generally, the plastic deformation of semicrystalline polymers is the result of several mechanisms of deformation of crystalline and non-crystalline phases [2–4]. Crystallographic slip, twinning, martensitic transformations, chains orientations and lamellar separation have been reported in uniaxial straining in common semicrystalline polymers. The deformation of PA11 have been studied by several authors in a number of deformation modes including solid-state uniaxial extension, equibiaxial deformation by forging [5], and shear deformation [6].

An important microstructural parameter of the crystalline part is the crystallographic texture, i.e. the distribution of the crystal lattice orientations. Due to the different types of bonding in polyamide, especially in PA11, a strong anisotropy (for which no precise information is known about up today) is expected. It is well known that many properties, first of all the mechanical properties, are directly linked to the crystallographic texture and the microstructure. The crystallographic texture is highly sensitive to the

* Corresponding author. Tel.: +33-3-87-31-53-95; fax: +33-3-87-31-53-77.

E-mail address: tidu@letam.sciences.univ-metz.fr (A. Tidu).

0032-3861/02/$ - see front matter
PII: S0032-3861(02)00486-X

anisotropic properties of polyamides. Consequently, the texture is essential to explain the plastic deformation. There is also a great interest in understanding the evolution of the texture according to thermal and to mechanical treatments.

The pole figures, which are used for texture evaluation, are the representation, in a stereographic projection, of the number of diffraction planes as a function of their orientation within the sample. The orientation of the crystallographic axes of the crystallites in a polycrystalline sample is defined in a three-dimensional macroscopic frame generally associated to the sample. In the case of semicrystalline polymers, the measurement and the analysis of pole figures are quite difficult because these materials are constituted of several phases. The X-ray lines associated to each phase are generally overlapped and the X-ray diffraction patterns must be analysed by using a fitting procedure in view to separate the contribution of each phase. The application of this method give, not only the intensity of a given reflection, but also all the other parameters of the X-ray line such as the 2θ position or the width 2ω. These parameters are generally associated to the microstructural state of the sample (residual stress, plastic deformation, disorder, etc.). Making this for all the position of the pole figure, we can obtain generalised pole figures (GPF) which are used to describe the microstructure in function of the orientation [7,8]. One of the first application of this method in the field of polymer sciences was probably the work of Galeski et al. [9].

To complete the microstructural observations, small angle X-ray scattering (SAXS) is used to obtain information at the mesoscopic level of the polymer: the packing and the orientation of the lamellae.

An important process that affects deformation of polymer is the relaxation process. This process starts when the load is taken off the sample or when the sample is loaded. The resulting microstructure can be greatly affected in terms of crystallographic texture, residual strain and microstrain, and packing of the lamellae.

In view of obtaining a better understanding of the texture and microstructure of polyamide PA11, this paper presents results obtained for samples subjected to a small uniaxial extension ($\varepsilon < 0.4$) by using WAXS and SAXS measurements carried out during in situ deformation. Therefore, the results reported in this study correspond to texture and microstructure 'under extension' in the sample.

2. Experimental methods

2.1. Materials and sample preparation

The material used in this study was Polyamide 11 (Rilsan Besno TL®, Atofina). The density is 1.03 g cm^{-3}. The glass transition temperature T_g, measured by differential scanning calorimetry (DSC), is about 40 °C.

The polyamide pellets were first dried under vacuum at 100 °C for 5 h. A mold is filled up with these pellets and is positioned between two metallic plates lined with aluminium foils that are covered with PTFE lubricant. Samples were prepared by compression moulding in a press at a temperature of about 210 °C and a pressure of 100 bar. Further, the cooling rate is about 5 °C/min. Fig. 1 displays the time–temperature–pressure used for our samples. The tensile specimens were 150 mm long and were punched out from the obtained 1 mm thick plates. Their working width is 12 mm. All these preparations were achieved in Institut Français du Pétrole (IFP, Rueil–Malmaison, France). No variation of the elastic moduli and Poisson ratio were observed according to the sampling direction from the plates.

The melting temperature of the quenched specimens is 190 °C as measured using a TA Instruments modulated DSC calorimeter at 2 °C/min. The degree of crystallinity of the as prepared sample is about 30% (measured by DSC). For similar materials, the amorphous phase presents different forms and it can be divided into two parts: the interlamellar and interspherulitic amorphous phase. The first represents approximately 25 vol% and the second one 75 vol% of the total amorphous phase [10].

Several ordered phases of polyamide PA11 have been observed and proposed by different authors. The α crystalline form is obtained by a different way: annealing of a quenched PA11, from crystallisation of the melted polymer [11] or from casting of a *m*-cresol solution [12]. The α′ form is obtained from melt-crystallisation [11]. The δ condis-crystal form results from thermal crystal transformation of α form above 90 °C [13]. The δ′ smectic form arises from melt quenched [14]. The γ crystalline form results from solvent casting from trifluoroacetic acid [15,16].

The α and α′structures have triclinic unit cells. The latter three forms (δ, δ′ and γ) are pseudo-hexagonal: a hexagon is described when unit cell is projected onto a plane

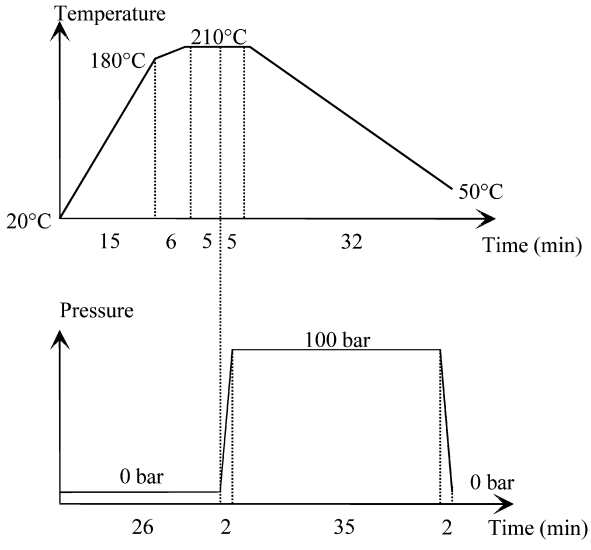

Fig. 1. Pressure–temperature time dependence.

perpendicular to the chain axis. But it should be stated that there is a lot of disagreements on crystal structure parameters for all these phases. Previous studies using modulated DSC calorimetry and WAX measurements have shown unambiguously the presence of the α-triclinic phase and of the δ′-pseudo-hexagonal one in our samples moulded by compression [17]. This result is in accordance with the earlier work [18] for similar PA11 moulded by compression. The δ′-pseudo-hexagonal crystal structure is virtually identical to the high temperature phase δ. The main difference is that the hydrogen bonds are dynamically and randomly oriented along and between the chains [14].

In our case, the lattice parameters of the triclinic α crystalline phase, calculated by using BIOSYM® software [19], are $a = 9.46$ Å, $b = 5.35$ Å, $c = 15.17$ Å, $\alpha = 52.2°$, $\beta = 80.4°$, $\gamma = 63.5°$. Fig. 2 shows the location of the main crystallographic planes. The polymer chains lie parallel to the *c*-axis, [001] direction, with strong covalent bonds along the chain, weaker Van der Waals bonds and strong hydrogen bonds between the chain segments. The alpha triclinic crystalline phase constitutes the lamellae of the spherulite. These lamellae are formed by a stack of (010) plane perpendicular to the radius of the spherulite [20].

According to microscopic observation, all the standard samples exhibit a spherulitic morphology in which the spherulites fill the entire volume. The mean diameter of the spherulites is about 20 μm.

2.2. Mechanical tests

The uniaxial extensions were carried out using a Zwick 1484® tensile machine. The standard samples in this study were deformed at ambient temperature, at an extension rate of $10^{-4}\,s^{-1}$ ($\pm 0.4 \times 10^{-4}\,s^{-1}$), to nominal (true) strain level of 0.02(0.02), 0.05(0.049), 0.1(0.095), 0.15(0.14), 0.20(0.182), 0.25(0.223) and 0.40(0.336).

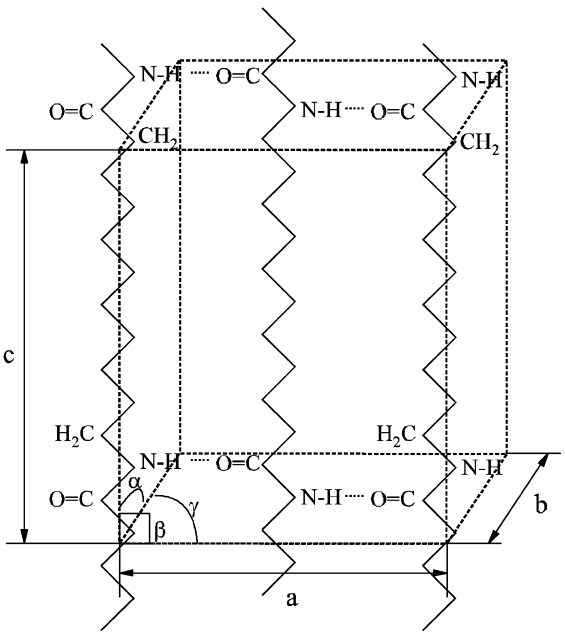

Fig. 2. Triclinic PA 11 cell [19].

For each strain level of interest, to ensure that any relaxation processes alter the measurement, the samples are kept under strain on the tensile machine during 25 min. After this time, a special device is attached to the sample that is always at the extension level fixed on the tensile machine. This device with the maintained sample is removed from the tensile machine and placed directly in the X-ray goniometer.

For the different level of strain, new samples are used. For the SAXS measurement, the same sample was used during the mechanical test.

2.3. X-ray diffraction and diffusion

Wide-angle X-ray diffraction (WAXD) measurements were carried out by transmission on a texture goniometer [21] equipped with a curved position sensitive detector (CPS120, Inel). The X-ray diffraction patterns were obtained using monochromatic Fe Kα radiation ($\lambda = 1.9373$ Å) with a graphite monochromator. The diffraction data were corrected for geometric absorption in the transmission case and for background using standard procedures.

The SAXS patterns were measured by using another system. The Cu Kα radiation ($\lambda = 1.5418$ Å) is emitted by a rotating anode Rigaku RU200 and filtered by an Ni absorption filter. The diffused beam was also collected by a curved position sensitive detector. The diffusion data were also corrected by using standard procedures.

In the case of WAXD measurement, according to a method described elsewhere [7–9], for each position of the pole figure, all the peaks of the X-ray diffraction patterns are analysed in view to obtain their descriptive values such as the full-width at half maximum 2ω, the position of the maximum 2θ, the integrated intensity. According to the work of Murthy et al. [22], it can be argued that the contribution of the thermal diffuse scattering (TDS) can be ignored because of its weak contribution to the amorphous phase. Such errors do not appear to affect the conclusions drawn in the discussion part of this paper.

After some preliminary studies, the Gaussian function, among all other tested functions, were found to describe adequately the diffraction peaks in the transmission geometry. Using these generalised pole figures for both the crystalline part and the non-crystalline part of the sample, we can follow the evolution of the different phases according to the imposed deformation.

In view to obtain the crystallographic texture, with a triclinic crystal structure, it is necessary to use at least three complete pole figures using the vector method [23] and $(2p + 1)$ complete pole figures (where p lies generally between 16 and 22) by using the generalised harmonic method [24]. The theoretical X-ray diffraction pattern of the crystalline α phase is calculated according to the lattice

parameter given above. The theoretical and a typical WAX pattern are displayed in Fig. 3. The overlapping of the different peaks of the crystalline and non-crystalline phases is observed. It is clearly seen, that in our case, only three independent and incomplete pole figures can be measured by X-ray diffraction. It should be clear that the texture cannot be described by using the methods mentioned. But the evolution of some parameter can describe qualitatively the evolution of the texture for uniaxial extension. These parameters are associated with the experimental method used. In the case of SAX method, an orientation factor of the lamellae, the so-called Hermann's factor [25,26], is defined as

$$f_1 = \frac{3\langle\cos^2\Phi\rangle - 1}{2}$$

where

$$\langle\cos^2\Phi\rangle = \int_0^{\pi/2} P(\Phi)\sin\Phi\cos^2\Phi\,\mathrm{d}\Phi \text{ and}$$

$$P(\Phi) = \frac{\int_0^{\infty} I(q,\Phi)q^2\,\mathrm{d}q}{\int_0^{\infty}\int_0^{\pi/2} I(q,\Phi)q^2\sin\Phi\,\mathrm{d}\Phi\,\mathrm{d}q}$$

In this expression $I(q,\Phi)$ is the diffracted intensity at the reciprocal point q in the direction Φ, Φ being the angle between the plane of the lamellae and the loading axis. $P(\Phi)$ represent the lamellar orientation distribution function. Because the function f_1 averages the lamellar orientations over the entire spherulite, it contains less information than $P(\Phi)$. For a set of (hkl) planes of a crystalline phase, the orientation function expressed as $f_1(hkl)$ is calculated using similar equation as those presented above.

The width of the amorphous halo is governed by many convoluted microstructural parameters such as the finite size of the domain, micro-strain in the domain and by the irregular packing. As it was pointed out in the introduction, polyamide PA11 presents two different amorphous components for which none of the characteristics are precisely known. In our opinion, these two components could have very similar properties. Therefore, the X-ray diffraction pattern of these two components cannot be distinguishable.

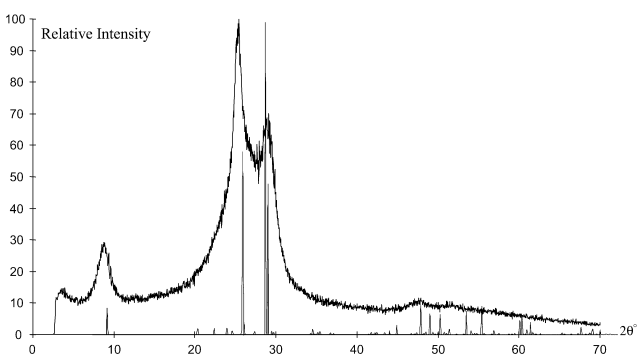

Fig. 3. Theoretical and typical WAX pattern measured.

Then, we consider only one component for the amorphous halo. The broadening of the amorphous halo must then be seen as a composition of the broadening associated to each of them. On the basis of Houseman's paracrystal model, the separation of size domain, order and micro-strain in the domain is possible in principle, however, this method is not used in this study. To take into account the results obtained for the amorphous phase, the amorphous line can be studied and simulated according to the method described by Murthy et al. [22]. This method consists of simulated WAX pattern diffused by an amorphous phase. This amorphous phase is described like a random arrangement of macromolecules with a given amorphous density η, the projection of each of them is a disk of diameter $2a$. The X-ray diffraction pattern of the amorphous phase is then calculated by using the two-dimensional arrangement of disks that gives an appropriate description of the packing of the polymer molecules. The analytical equations derived by Rosenfeld [27] are used. They are based on a free-energy model to calculate the interference function $S(q)$ at $q = 4\pi\sin\theta/\lambda$. According to the Rosenfeld's equations, the principal parameters of this function are the amorphous density η and the disk diameter $2a$. The width and the position of the amorphous halo depend on both parameters.

The changes in both the lamellar orientation and long period were studied by means of SAXS measurements. These measurements are carried out also for samples subjected to uniaxial extension.

3. Results and discussion

3.1. Microstructure analysis

3.1.1. Preliminary studies

The theoretical diffraction pattern (Fig. 3) shows that the (010) line is very close to the (210) one. Owing to broadening of peaks, these two peaks are necessarily overlapped on the measured XRD patterns. Then, only one peak is considered in the fitting procedure to describe both lines. This doublet line is called {(210); (010)}. This rough approximation does not affect the result concerning the evolution of the texture as it is demonstrated further. Considering the geometrical path of the incident beam, the peak located under 12° (2θ) is greatly affected by the X-ray diffusion in air although the diffusion knife and absorbing mask are located in front of the detector. Then, in this paper, our interest is only on peaks located in the 12–43° (2θ) range.

Our aim is to characterise the main features of the texture of the standard and deformed samples. The measurement direction is defined in the sample co-ordinate system and it is located by the point P having (φ_m, ψ_m) as co-ordinates on a stereographic projection (Fig. 4). In this figure, the intersection of the crosshairs corresponds to the loading direction (the DL-axis), while the DT-axis represents

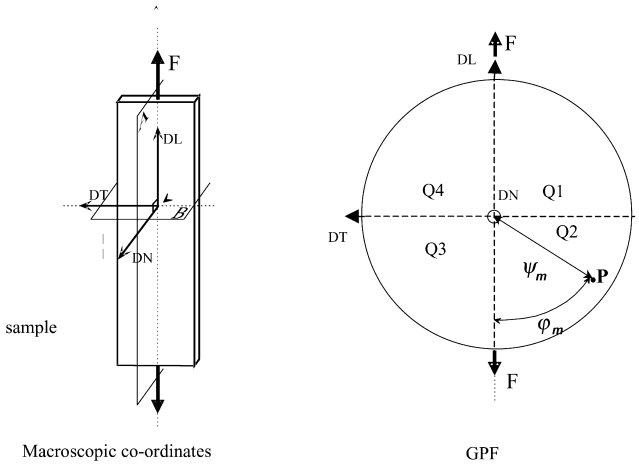

Fig. 4. Macroscopic co-ordinates and GPF.

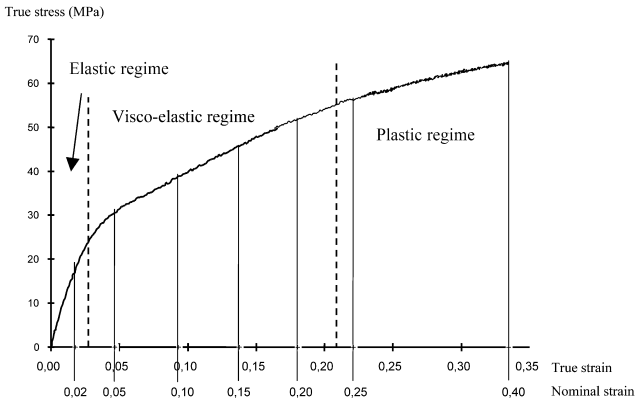

Fig. 5. Stress–strain curve.

transverse direction, the DN-axis the normal direction. The macroscopic processing and the shape of the samples imply two macroscopic symmetries, which are perpendicular to the sample plane, respectively, parallel and perpendicular to DL. For the non-deformed sample, according to the moulding radial symmetries, only one-half meridian line ($0 \leq \psi_m \leq 90°$) and one radius ($0 \leq \varphi_m \leq 90°$) of the pole figure must be measured. Then, it seems that, in the general case of a deformed or non-deformed sample, the measurement of a quarter of the pole figure must be representative of the whole pole figure.

To assert these last assumptions, measurements of the pole figure were performed in two quarters (Q1 and Q2 in Fig. 4) for a non-deformed sample and deformed samples. In each case, the grid of measurement were: $0 < \varphi_m < 180°$ (step 10°), $55 < \psi_m < 90°$ (step 5°). For each point of the grid, the diffraction pattern is measured and analysed according to the method presented above.

The results of the analysis for a non-deformed sample show that, for all the peak analysed, all the calculated parameters are nearly constant in function of the angle φ_m. However, the variation of the peaks areas in function of the decline angle ψ_m are quite different for both phases. The peak area of the amorphous halo and of the characteristic δ' are nearly constant. On the other hand, the areas of the peaks of the crystalline phase vary weakly indicating that, after crystallisation from the melt in the mold, the crystalline phase presents a preferred orientation [17]. These variations show that the crystalline cells are weakly oriented with the crystallographic plane containing the hydrogen bonds parallel to the sample, i.e. the H-bondings plane perpendicular to the pressure direction. This kind of texture has already been observed by Galeski et al. [28] for polyamide PA6. This weak tendency is neglected in the following: we assume that the standard samples are isotropic [28] as is to be expected regarding thier process of fabrication [1].

The sample were subjected to the nominal (true) uniaxial strain: $\varepsilon = 0.02(0.02)$, $0.05(0.049)$, $0.1(0.095)$, $0.15(0.14)$, $0.20(0.182)$, $0.25(0.223)$ and $0.40(0.336)$. The stress–strain curve for uniaxial extension is depicted in Fig. 5. This curve presents an initially linear elastic regime and a viscoelastic one with different modulus before necking occurs which marks the beginning of the plastic deformation. These different behaviours are marked in Fig. 5. The initial elastic regime extends up to a strain of about 0.05 and is followed by the viscoelastic regime up to $\varepsilon = 0.2$ and by the plastic regime flow from yield point to the fracture, yield occurring at 55 MPa (as shown in Fig. 5).

Concerning these deformed samples, we present the complete results for a true strain of $\varepsilon = 0.18$. The whole pole figures of Fig. 6 (peaks area), Fig. 7 (peaks position) and Fig. 8 (peaks width) are obtained by applying a (DN, DL) planar symmetry. The pole figure is characteristic of a fibre texture whose axis of symmetry is the loading direction (DL). The same cylindrical axis is observed for all the other measured generalised pole figure. This last point was confirmed by the measurement of diffraction patterns along different meridian lines (i.e. Wulff meridian). The angles between the three meridians and the (DN, DL) plane are respectively, 60, 75 and 90° for azimutal angle φ_m from 0 to 180° each 10°. The results of these analysis show that all the calculated parameters are equal in function of the tilting angle ψ_m.

This shows that the texture of the different phases of samples subjected to an uniaxial strain has a cylindrical symmetry axis: the loading direction. Therefore, the texture and microstructure measurements can be achieved only by the measurements on a meridian line of the pole figure. In the following, all the measurements are made along the meridian line defined by $\psi_m = 90°$ and for a step scanning of the azimutal angle of $\Delta\varphi = 10°$.

3.1.2. Mesoscopic scale (SAX studies)

On the basis of the recorded and corrected SAX intensities, the long periods $L(\Phi)$ and the lamellar orientation distribution $P(\Phi)$ from the loading direction to the direction perpendicular to it (i.e. from meridian to equator) were calculated for the standard and deformed samples. The angle Φ is the angle between the loading direction and the plane of the lamellae. The direction of

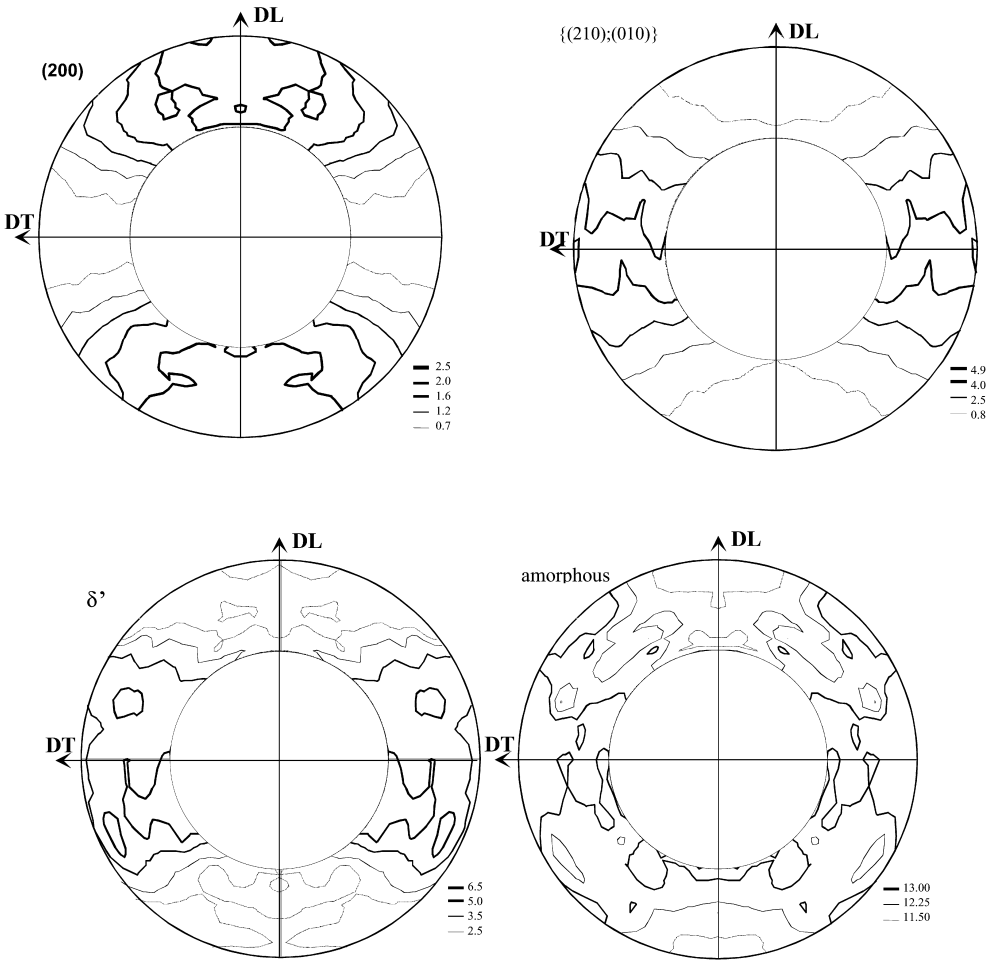

Fig. 6. GPF of areas (arbitrary units) of peaks located in 12–43° range. Whole GPF are obtained by applying a (DN, DL) planar symmetry.

measurement in the sample are $\Phi = 0$, 15, 30, 45, 60, 75 and 90° and the nominal (true) uniaxial strain are $\varepsilon = 0$, 0.05(0.049), 0.10(0.095), 0.160(0.155) and 0.240(0.214).

Fig. 9 displays the variation of $P(\Phi)$ in function of the true strain and of the direction in the sample. For the undeformed sample, the lamellar orientation distribution function is the same for all angle Φ indicating an isotropic sample. For all true strains, the lamellar orientation function at $\Phi = 0$ is greater than that at $\Phi = 90°$. The greater the value of the lamellar orientation distribution function, the higher the probability of finding lamellae at an angle Φ. This phenomenon indicates that as the strain increases, the number of lamellae parallel to the loading axis increases, while that perpendicular to the loading axis decreased. This phenomenon is well known and has been reported by many workers [26,30].

For each of the strain levels, the orientation lamellar function f_l is calculated. Fig. 10 depicts the obtained results. Generally the f_l factor is displayed from $f_l = -1/2$ (i.e. all the lamellae perpendicular to the loading direction) to $f_l = 1$ (i.e. all the lamellae parallel to the loading direction). The results show that the lamellae tend to be oriented parallel to the loading direction. However, this low level of the orientation factor f_l indicates that the orientation of the lamellae is not far from isotropic.

The variations of the long period according to the true strain and to the direction in the sample are presented in Fig. 11. As shown in the figure, the long period, as measured in the meridian direction, (i.e. lamellae perpendicular to the loading direction) steadily increases with increasing strain, whereas in the equator direction (i.e. lamellae parallel to the loading direction) the opposite behaviour is observed. For all values of the strain, the long period decreases from the meridian to the equatorial direction. The decrease of the long period for lamellae parallel to the loading direction can be well explained by the lamellar sliding (shear). The increase of the long period for the lamellae perpendicular to the loading direction reflects the lamellar separation, the result must be seen as a thickening of the amorphous layer between them or an extension of the lamellae. Other phenomenon, playing also a role in these processes, are commonly considered: lamellar bending, untwisting and chain tilting.

3.1.3. WAX studies of the non-crystalline phases

The non-crystalline phases are the amorphous and the

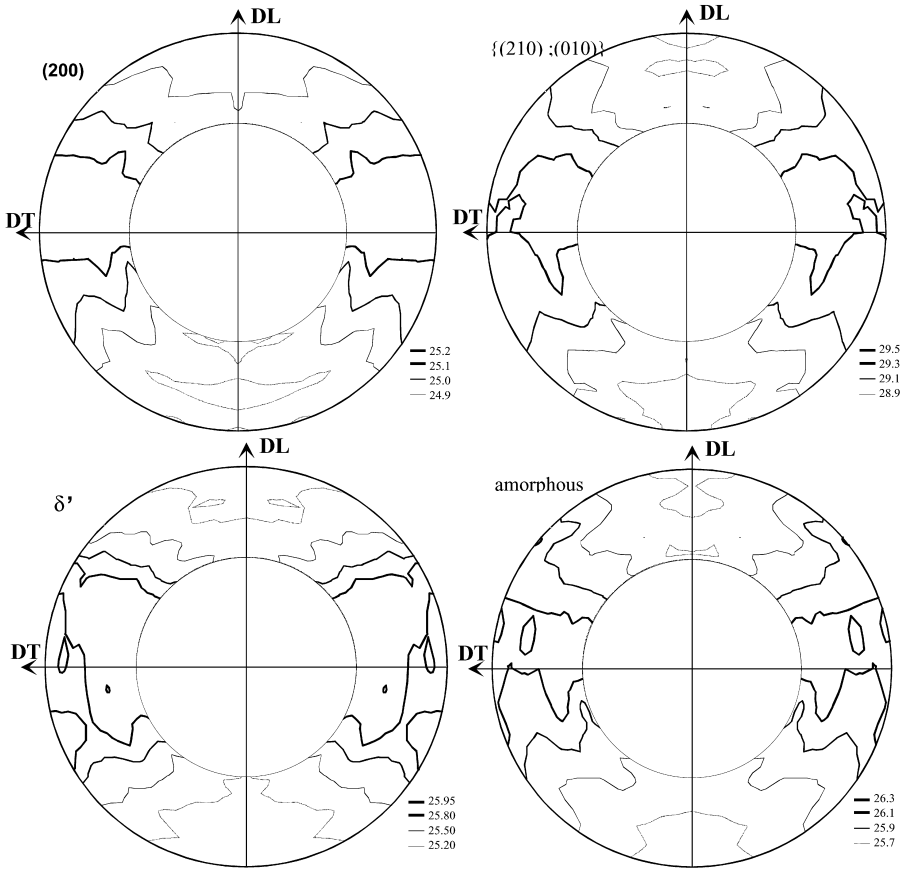

Fig. 7. GPF of positions (in degrees in 2θ) of peaks located in 12–43° range in 2θ. Whole GPF are obtained by applying a (DN, DL) planar symmetry.

smectic δ' phases. As it was pointed out above, all the descriptive values present a cylindrical symmetry axis, which can be seen as a fibre axis. The integrated intensity (i.e. the area under the peak) is directly linked to the diffusing matter. Therefore, the orientation of the chains is deducted from the variation of this area as a function of the direction in the sample. Fig. 12a and b shows that the variations of the area of both peaks show similar behaviour.

In the case of the non-deformed sample, for both phases, the area is constant in function of φ_m. For loaded samples, the areas present a maximal value at $\varphi_m = 90°$ (equator) and a minimal value at $\varphi_m = 0$ and 180° (meridian). We can notice that the variations of the area of the ($hk0$) peak of the δ' phase is higher than the amorphous halo one.

By summing all the X-ray diffraction patterns measured along the meridian line $\psi = 90°$, we conclude that the volumic part of the amorphous and smectic phase does not change according to the imposed strain. Therefore, the variations of the areas are only a function of the orientation of the chains. At the equator position ($\varphi_m = 90°$), the measured δ' crystallites have their chains parallels to the loading direction. Respectively, at the meridian positions ($\varphi_m = 0$ and 180° the measured crystallites have their chains perpendicular to the loading direction. From these observations, it is concluded that the chains of the smectic phase and of the amorphous phase tend to be weakly oriented parallel to the loading direction.

Fig. 13a and b shows, respectively, the variations of the position 2θ and of the integral width of the peak of the smectic phase. The integral width is linked to the macromolecular arrangement or to the crystallite size [29] and the 2θ position reflects the interchain distance. At the equator position, the average length between chains and the integral width is nearly constant for all imposed strains. At the meridian positions, the position of the peak and the integral breadth decrease according to the imposed strain. We suppose that these variations are linked to an increase of the average length between chains and of the packing order of the chains. This behaviour can be explained by the fact that the direction of the extension axis is perpendicular to these chains.

Fig. 14a and b shows that the position at which the maximum intensity was observed and the integral width of the amorphous halo in deformed samples depends on the strain and on the direction in the sample. These results suggest a high degree of ordering of the amorphous chains oriented along the DT direction. In order to characterise the arrangement of the chains in the amorphous phase, the simulation of the X-ray diffraction pattern described in Section 2.3 is used. The position and the integral width are closely linked with the density of packing η and a disk

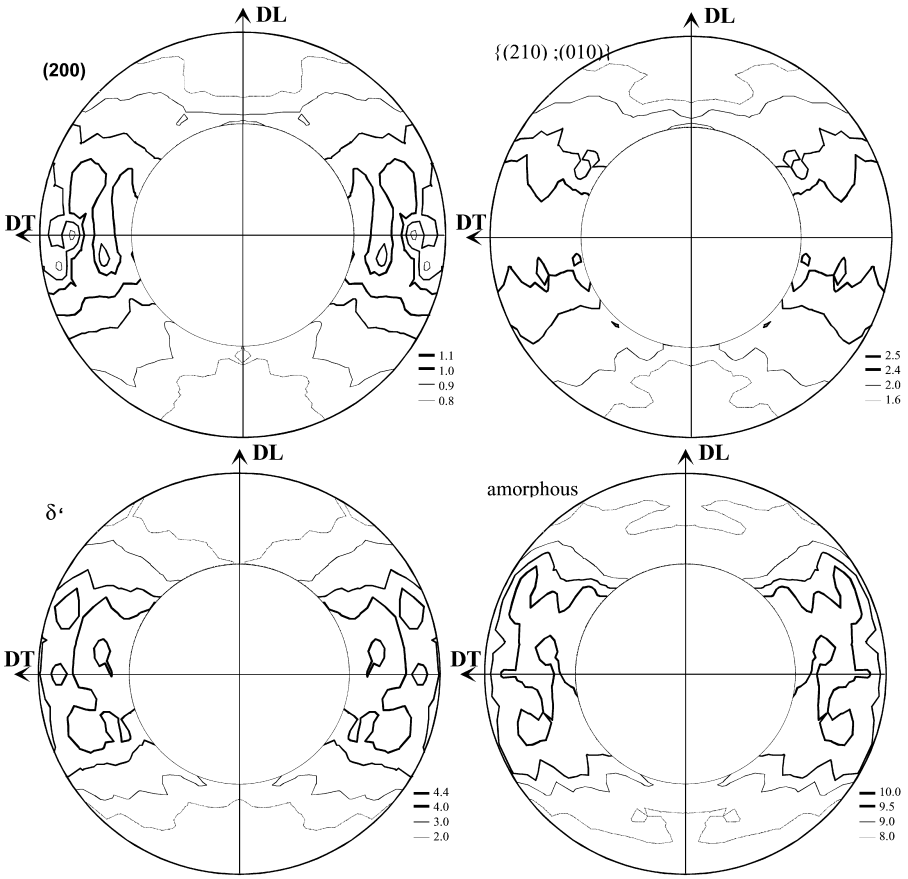

Fig. 8. GPF of width (in degrees) of peaks located in 12–43° range in 2θ. Whole GPF are obtained by applying a (DN, DL) planar symmetry.

diameter $2a$. In Fig. 15, the width and the peak position of the amorphous halo are plotted on a $2a-\eta$ grid. The theoretical grid is drawn using the width and the position of the amorphous halo calculated for disks of diameter 3.8, 4.0, 4.2 Å at densities 0.50, 0.55, 0.60. Using these points (filled squares) theoretical lines of constant diameter and constant density are drawn. The filled circles and triangles represent the values obtained at various levels of deformation, respectively, at the equator and the meridian positions. At the equatorial position, the density is nearly constant and the disk diameter tends to decrease. At the meridian positions, the density and the disk diameter tend to increase. Therefore, we conclude that the organisation of the chains oriented perpendicularly to the extension direction increase as a function of the deformation. No successful hypotheses can explain the variation of the disk diameter, linked directly to the radius of gyration of the chains. Among all hypothesis one could find an incomplete description of the scattering of the amorphous phase by taking into account only two parameters ($2a$ and η). At least, these observed variations can be explained by the reorientation of the chains during the imposed strain.

In conclusion, the behaviour of both non-crystalline phases are similar, though more pronounced for the smectic δ' phase. When the imposed extensional strain increases, the

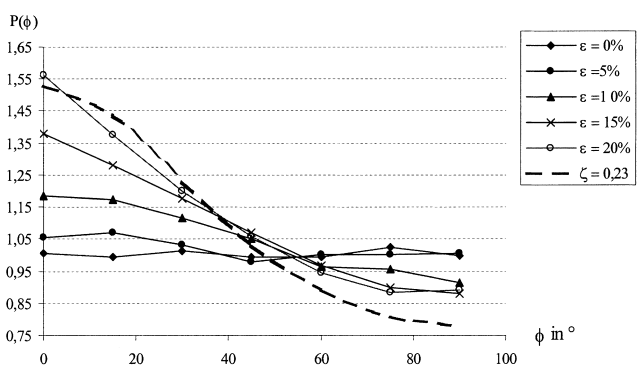

Fig. 9. Variation of $P(\Phi)$ according to Φ at constant nominal strain.

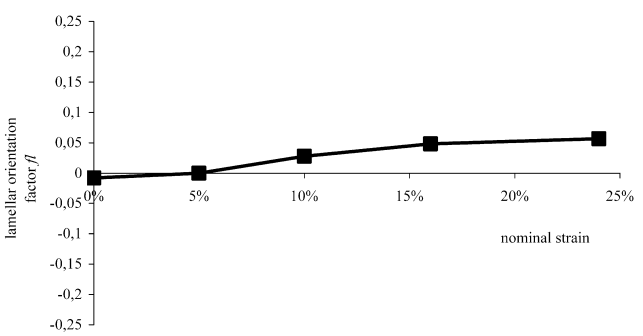

Fig. 10. Lamellar orientation factor in function of the nominal strain.

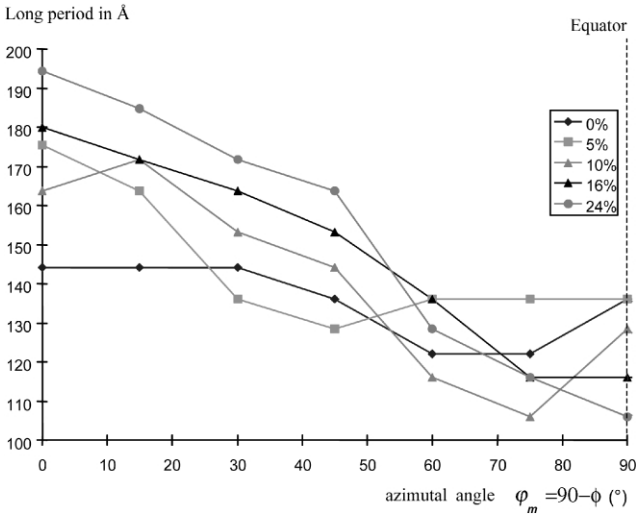

Fig. 11. Variation of the long period.

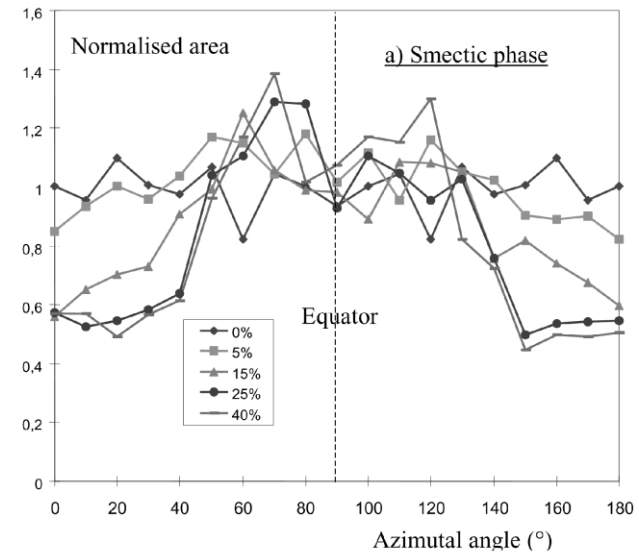

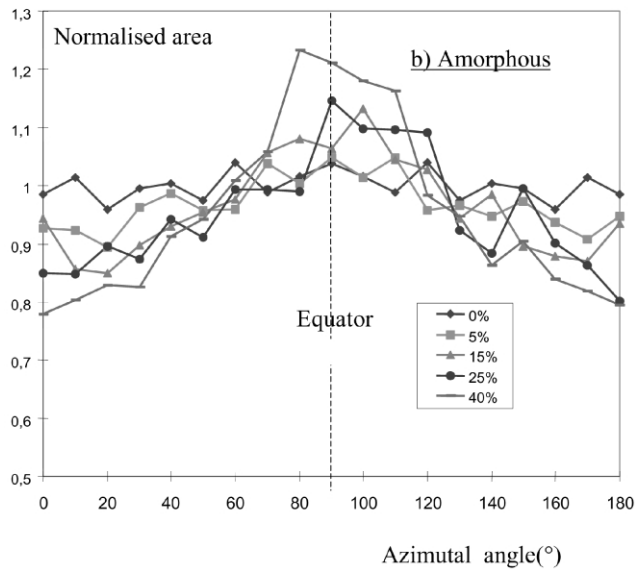

Fig. 12. Normalised area of (a) the smectic and (b) amorphous phase.

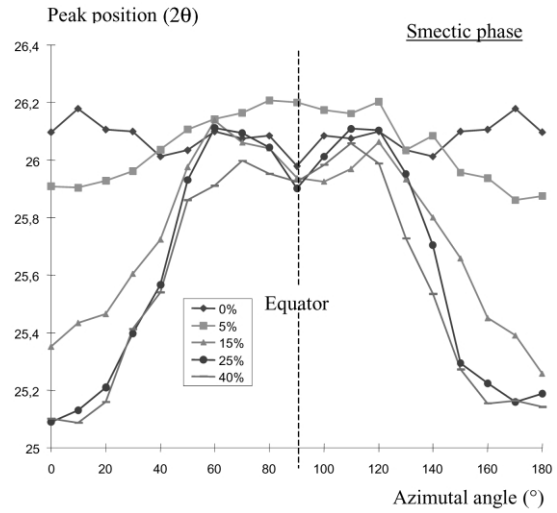

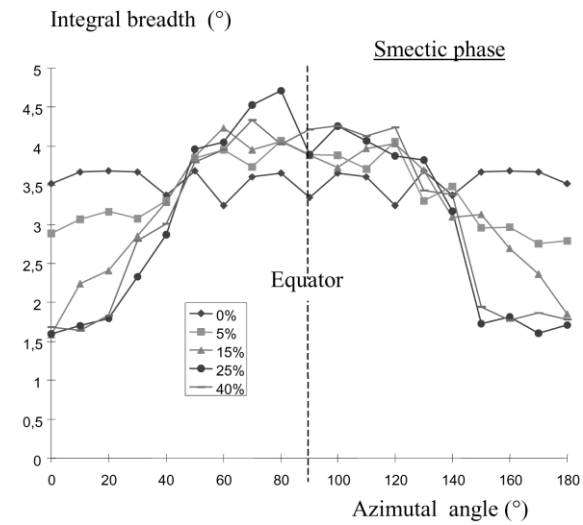

Fig. 13. Centroide (peak position) and integral breadth of the peak of the smectic phase.

chains tend to be oriented parallel to the extension direction. At the same time, the arrangement order of the chains, which are perpendicular to the extension direction tends to increase. This similar behaviour shows strong interaction between both phases. We suppose that the crystallites of the smectic phase are included in the amorphous phase. According to the high width of the peak of the smectic phase, the crystallite size can be supposed to be small in comparison with the dimensions of the lamellae. Probably, these crystallites can be seen as clusters or bundles [31] in the amorphous phase.

3.1.4. WAX studies of the crystalline phase

For the analysis of the crystalline α phase, we have three exploitable lines: (200), (010) and (210), more precisely the (200) and the doublet line. The orientation of the planes allows us to deduce the orientation of the chain segments from the knowledge of the unit cell. Fig. 16 shows that the area of the lines of the non-deformed standard sample is a

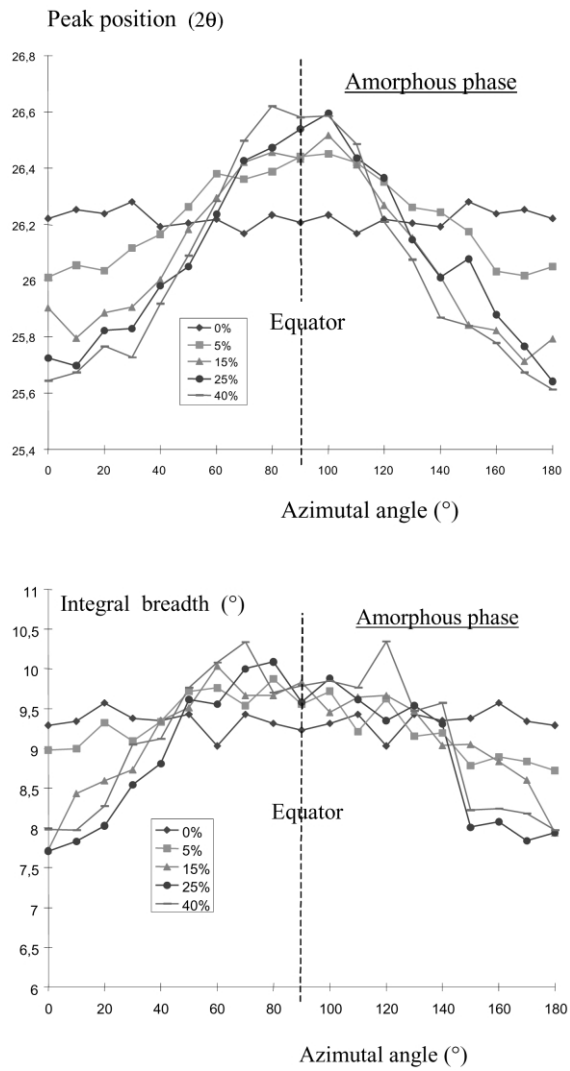

Fig. 14. Centroide (peak position) and integral breadth of the peak of the amorphous phase.

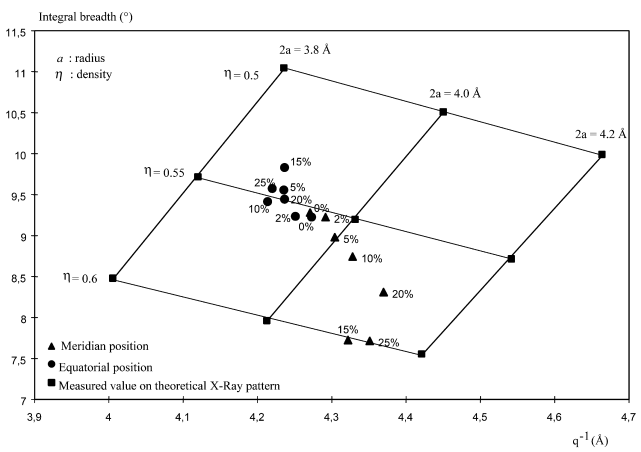

Fig. 15. Murthy's plot for the amorphous phase.

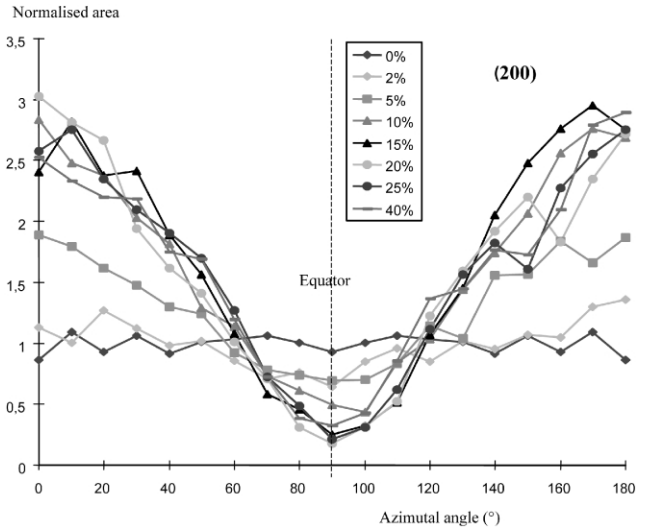

Fig. 16. Normalised area for the (200) pole according to the strain and the azimutal angle.

constant function of φ_m. During the extension, the area of the (200) peak decreases at the equator position and increases at the meridian positions until $\varepsilon = 0.095$. From $\varepsilon = 0.095$ to 0.336, the variation is much less pronounced. These variations show that the (200) planes tend to be oriented perpendicular to the extension direction principally at very low strains. Conversely, the variation of the area of the doublet line varies continuously until $\varepsilon = 0.336$: the area decreases at the meridian positions and increases at the equator position. We have stated that all the measured values present a cylindrical axis. The theoretical pole figure of a single crystal of polyamide PA11 with the (200) plane perpendicular to the loading direction shows that the (010) and (210) poles are close to the transverse direction (Fig. 17). Then, it can be argued that the (010) and (210) planes tend to be oriented parallel to the loading direction. Because these two planes have nearly the same tilt angle with respect to the loading axis, the variations of the

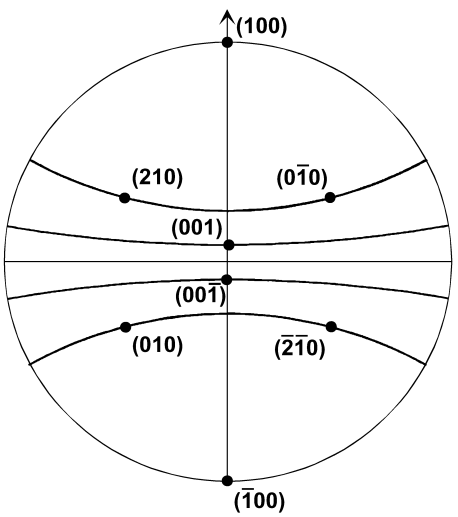

Fig. 17. Stereographic projection.

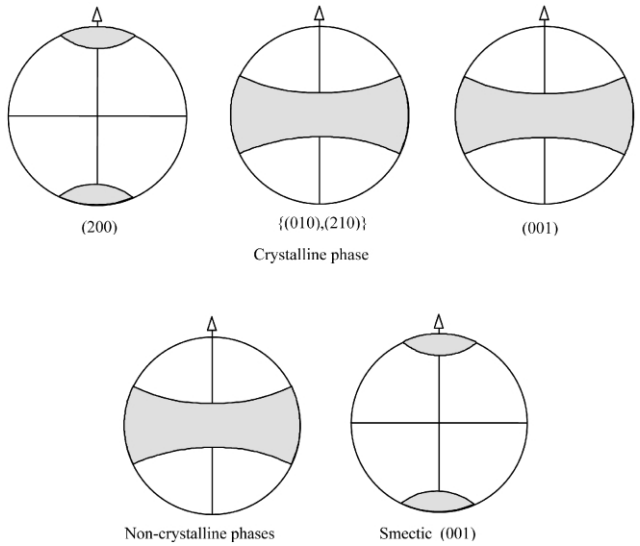

Fig. 18. Idealised pole figures after extension at 40%.

intensities of the doublet line {(010),(210)} are close to those of the (010) and (210) X-ray peaks taken individually.

All these variations of peak areas are higher than those observed for the non-crystalline phase. The main conclusion is that the chain segments of the crystalline phase are subjected to more reorientation than the one of the non-crystalline phases and that their orientation is opposite to that of the non-crystalline phase. These results obtained allow us to propose idealised representation of the pole figures of PA11 subjected to a small uniaxial strain. They are depicted in Fig. 18 together with the one of non-crystalline phases.

Using the data obtained for the 2θ angle of the X-ray line peak, Fig. 19 presents the variation of the interplanar spacing $d(200)$ of the crystalline α phase according to the macroscopic strain for three directions in the sample: the north and south-meridian and the equator directions. In this figure, the different regimes of deformation of the crystalline phase are clearly visible. In the initial stage, during the elastic regime, the interchain distance linked to the interplanar spacing $d(200)$ decreases at the equator and

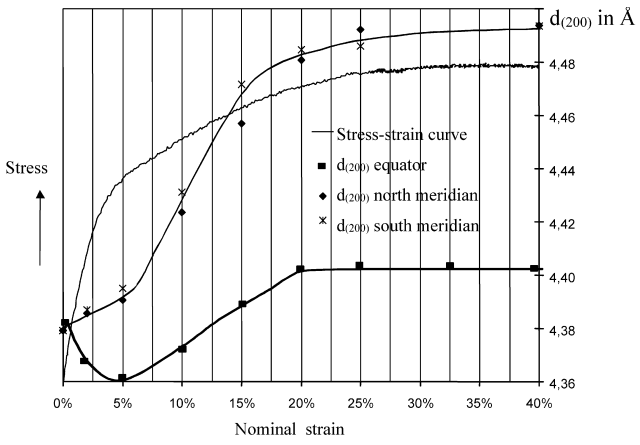

Fig. 19. Variation of the interplanar spacing according to the nominal strain.

increases at the meridian positions. During the viscoelastic regime, for both directions, the $d(200)$ increases until necking occurs. During the third section of the curve the $d(200)$ lattice distance remains nearly constant for all directions in the sample. At the beginning of the deformation the $d(200)$ are the same for the two directions, while at the end we have $d_{(200)}^{\text{equator}} < d_{(200)}^{\text{meridian}}$.

In our opinion, these variations are due to the elastic strain imposed to the crystalline phase during the mechanical test. To precisely understand these observations, a precise X-ray stress–strain analysis of the material is necessary and has to be promoted.

3.2. Deformation mechanism

It has been shown for semicrystalline polymers [32,33] that the deformation is not uniform. It depends mainly on the direction of the lamellae inside the spherulite with respect to the extension direction. In the equatorial zone of the spherulite, where the lamellae are nearly perpendicular to the loading direction, the interlamellar material is in extension. For the lamellae, which are parallel to the loading direction, the lamellae are expected to be in extension. For the other lamellae, i.e. for the remaining part of the spherulites, shear of both lamellae and in the interlamellar regions occurs providing an additional degree of freedom for plastic deformation. From a theoretical point of view, the deformation of spherulites was first considered as affine, i.e. all the region of the spherulite follows the strain of the bulk sample [34]. This model was successfully amended by Young et al. [26] by introducing the untwisting process. The twisting of the lamellae about the spherulite radius is defined by the parameter ζ which indicates the ease of lamellar untwisting. Such a model gives more complete information about the deformation of the lamellae under extension. In this model, the $P(\Phi)$ and f_1 are theoretically calculated introducing this untwisting parameter for the lamellae. The application of this model shows clearly that an untwisting process occurs in our sample. The result for $\zeta = 0.23$ is presented in Fig. 9. This process would predominate in the equatorial part of the spherulite where the applied strain is perpendicular to the lamellar axis [26]. This model does not take into account other phenomenon which are active in the crystallite part of the spherulite and the observed variation of $P(\Phi)$ is certainly not only due to this untwisting process.

In Section 3.2 we have proposed a model of a cluster or a bundle for the smectic phase. The great width at half maximum of the X-ray line suggests a small domain size, then this phase could be seen as formed of microcrystallites. This point can be compared to the work of Bélec [35]: during an experiment linked to creep under the glass transition temperature, the strain is directly linked to the interaction between the amorphous phase and microcrystallites (for which no specific descriptions were given). These microcrystallites act as obstacles in the progression of

shear bands in the amorphous phase during the deformation. In our opinion, the representation of the smectic phase like microcrystallite is a good way to explain this behaviour.

As it was pointed out above, the lamellae grow with (010) planes perpendicular to the radius of the spherulite. The changes in the lamellar orientation are accompanied by significant changes in crystal orientation and microstructure in terms of residual stresses and order. Then, according to the observed behaviour of the lamellae, we must observe a fibre axis with the (200) plane of the crystalline phase parallel to the loading axis. This point is in contradiction with the results of WAX studies, which implies the (200) plane perpendicular to the loading direction. Another point of high importance is the comparison of the orientation factors calculated for the lamellae and for the (200) peak according to the formula given in Section 2.3. These two curves must show the same behaviour because the lamellae contain all the crystalline phase. In Fig. 20, the orientation factors of both the lamellae and the (200) plane are presented. As it is seen in this figure, the two curves spreads out between $\varepsilon = 0.02$ and 0.05. These orientation factors reach their limit value at $\varepsilon = 0.10$. Among all deformation mechanisms observed in spherulitic semi-crystalline polymer, twinning was observed in the case of PA6,6 [32] and suspected in PA11 [5]. The twinning process leads to a significant modification of the lattice in the case of PA6,6 (which is very close of PA11 according to their mechanical and physical properties). In the case of PA6,6 this twinning produces a drastic orientation effect. Twinning is operative when the chains are perpendicular to the loading direction and appropriately oriented for twinning. The twinning deformation mode is presented in Fig. 21. We can see from this figure that the twinning plane is the (210) plane and that the (200) plane undergoes a great reorientation. If we suppose that this twinning operates in the case of PA11, the results presented in the preceding discussion are in good correlation: the increase of the number of (200) plane perpendicular to the loading direction is then compatible with the orientation of the lamellae.

When the orientation factors have reached their limit all the lamellae correctly oriented have twinned (Fig. 20). This means that the (210) twinning process is mainly operative during the viscoelastic regime and that plastic deformation starts with twinning.

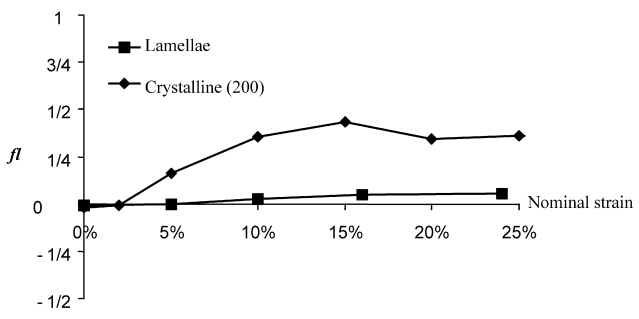

Fig. 20. f_l factor for the lamellae and the (002) plane.

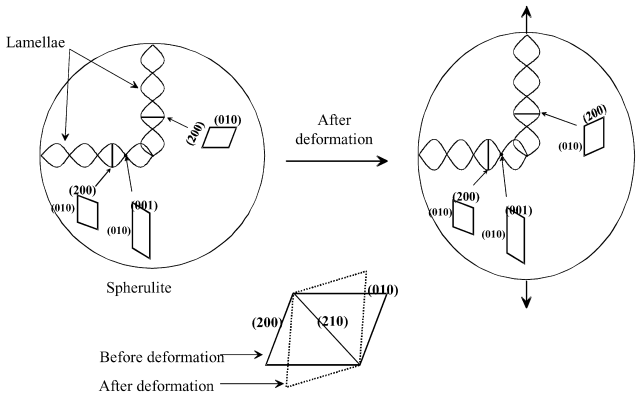

Fig. 21. Twinning mechanism during the orientation of lamellae [30].

4. Conclusions

The experimental results discussed in this paper show that the deformation of semicrystalline polyamide PA11 in uniaxial extension induces a preferred orientation of macromolecules, not only for the crystalline part, but also for the non-crystalline phases.

For these non-crystalline phases, the chains are aligned along the loading direction. These observations are linked to the deformation, which occurs mainly by sliding and lamellar separation. As a result, the packing density varies according to the direction in the sample.

For the crystalline phase, a (210) twinning process occurs during the viscoelastic regime: the (200) planes are perpendicular to the loading direction. Also, an untwisting process occurs at low strain.

Acknowledgments

The authors would like to acknowledge the support from the Institut Français du Pétrole (IFP-Reuil Malmaison), especially Dr Y. Meimon and Dr F. Dal Maso for helpful discussions. We are indebted to Dr L. Barre and C. Cairati from IFP for SAX measurement facilities.

References

[1] Li D, Garmestani H, Kalidinda SR, Alamo R. Polymer 2001;42:4903–13.
[2] Aboulfaraj M, G'sell C, Ulrich B, Dahoun A. Polymer 1995;36(4):731–42.
[3] Avramova N. Polym Polym Compos 1993;1(4):261–74.
[4] Bowden PB, Young RJ. J Mater Sci 1974;9:2034–51.
[5] Autran JP. PhD Thesis. University of Massassuchets, USA; 1990.
[6] Dosiere M, Point JJ. J Polym Sci: Polym Phys Ed 1984;22:1383–98.
[7] Tidu A. PhD Thesis. University of Metz, France; 1991.
[8] Wcislak L, Bunge HJ. Texture analysis with a position sensitive detector. Göttingen: Villier; 1996.
[9] Galeski A, Argon AS, Cohen RE. Macromolecules 1991;24:3945–52.
[10] Serpe G, Chaupart N. J Polym Sci: Polym Phys 1996;34:2351–65.
[11] Slichter WP. J Polym Sci 1959;36:259–66.

[12] Kim KG, Newman BA, Scheinbeim JI. J Polym Sci: Polym Phys Ed 1985;23:2477–82.
[13] Newman BA, Sham TP, Pae KD. J Appl Phys 1977;48:4092–8.
[14] Mathias LJ, Powell DG, Autran JP, Porter RS. Macromolecules 1990; 23:963–7.
[15] Sasaki T. Polym Lett 1965;3:557–60.
[16] Kawaguchi A, Ikawa T, Fujiwara Y, Tabuchi M, Konobe K. J Macromol Sci: Phys 1981;B20(1):1–20.
[17] Jolly L. PhD Thesis. University of Metz, France; 2000.
[18] Chen PK, Newman BA, Scheinbeim JI, Pae KD. J Mater Sci 1985;20: 1753–62.
[19] Dal Maso F, Toulhouat H. Private communication IFP; 1996.
[20] Magill JH. J Polym Sci, Part A-2 1969;7:123–42.
[21] Heizmann J-J, Laruelle C, Vadon A. Analysis 1986;16:334–40.
[22] Murthy NS, Minor H, Bednarczyk C, Krimm S. Macromolecules 1993;26:1712–21.
[23] Vadon A. PhD Thesis. University of Metz, France; 1983.
[24] Bunge HJ. Zeitung metalkunde 1965;56:872.
[25] Hermans JJ, Hermans PH, Vermaas B, Weidinger A. Recueil de travaux de Chimie 1946;65:427–47.
[26] Young P, Stein RS, Kyu T. J Polym Sci: Polym Phys 1990;28: 1791–812.
[27] Rosenfeld Y. Phys Rev A 1990;42(10):5978–89.
[28] Galeski A, Argon AS, Cohen RE. Macromolecules 1991;24:3953–61.
[29] Hosemann R, Baghi SN. Direct analysis of diffraction by matter. Amsterdam, The Netherland: North-Holland; 1962.
[30] Hay IL, Keller A. J Mater Sci 1967;2:538–58.
[31] Sasanuma Y, Abe A, Sasanuma T, Kitano Y, Ishitani A. J Polym Sci, Part B: Polym Phys 1993;31:1179–86.
[32] Hay IL, Keller A. J Polym Sci, Part C 1970;30:289–96.
[33] Samuels RJ. J Appl Polym Sci 1981;26:1383–412.
[34] Wilchinsky ZW. Polymer 1964;5:271–81.
[35] Bélec L. PhD Thesis. University of Poitiers, France; 1995.